Computational simulation of Haidinger's Brushes

GARY P. MISSON[1, 2*], SHELBY E. TEMPLE[3], STEPHEN J. ANDERSON[2]

[1]South Warwickshire NHS Foundation Trust, Warwick Hospital, Lakin Road, Warwick, CV34 5BW, UK
[2]School of Life and Health Sciences, Aston University, Birmingham, B4 7ET, UK
[3]School of Biological Sciences, University of Bristol, Bristol, BS8 1TH, UK
*Corresponding author: garypmisson@gmail.com

Haidinger's Brushes (HB) are entoptic phenomena resulting from differential absorption of linear polarized light by the human macula. Computational models have assisted in understanding the behaviour of these subjective phenomena, but have been limited in their application. This study presents a revised computational model that incorporates known determinants of the form and behaviour of HB. The model generates both static and animated simulations of HB that can be quantified by their density, contrast and radial/circumferential extent. Measured physiological parameters are used to demonstrate the dependency of HB on macular pigment (MP) density, MP distribution and ocular retardation. Physiological variations in these parameters explain the reported variations in the perception of HB.

© 2018 Optical Society of America

1. Introduction

The entoptic phenomenon of Haidinger's brushes [1] (HB) is a manifestation of the human eye's ability to detect linear polarized light [2]. The brushes are perceived by most humans with normal vision when observing a uniform field of linear polarized light. Observed with white polarized light, they appear as a faint yellow hour-glass like image radiating 1 – 4° from the point of fixation. Blue areas between the yellow brushes [3] are most likely a secondary effect of yellow-blue colour opponent neural processes [4, 5]. HB fade after several seconds [6] due to retinal adaptation, but a persistent image is obtained by rotating the plane of incident polarization, in which case the brushes typically appear to rotate in the same direction. Variability in HB orientation direction and contrast throughout a rotation is influenced by the intrinsic optical retarding properties of the cornea [7, 8] and externally placed optical retarders [9].

The accepted explanation for HB is that they are generated by differential absorption of polarized light by radially arranged pleochroic elements within the macular retina [10, 11]. The dependence of HB on intact macular anatomy has led to their clinical use for the detection of eye disease in which there is macular dysfunction (e.g. age related macular degeneration) [12-14]. The strong association between HB and macular pigment [5, 15, 16] has led to recent quantitative investigations of HB [17] as a possible index of macular pigment density. This renewed interest in HB as a potential clinical test highlights the importance of understanding the properties of the phenomenon in both health and disease.

The entoptic nature of HB means that it cannot be imaged objectively: any pictorial representations are typically artistic impressions, the most accurate of which are probably those of Haidinger's original paper [1]. Furthermore, the phenomenon is faint and perceived differently between observers [11]. Theoretical models have therefore been a convenient way of exploring the form and behaviour of HB and in advancing understanding [18-20]. To date, these models have assumed the macula has perfect radial symmetry, there is complete absorption of polarized light (full diattenuation), and that there is no spatial variation in the ability of the macula to absorb polarized light.

The present study refines earlier models by incorporating components that represent the spatial distribution and absorptive properties (diattenuation) of radially orientated pleochroic macular elements. Variations in the morphology of HB are simulated using density functions relevant to known experimentally-determined macular pigment distributions. The utility of the model is also demonstrated by static and animated dynamic simulation of the effect of physiological values of ocular retardation.

2. Theory and Methods

The theory of HB is concisely described using Mueller matrix transformations of the Stokes' vector representation of polarized light

[19]. The components (Stokes' parameters) of the Stokes' vector $\mathbf{S}$ = $(S_0, S_1, S_2, S_3)^T$ describe the polarization state of monochromatic light. The properties of optical components with respect to polarized light, including those of the eye [21], are defined by standard Mueller matrices [22-24]. The polarization output expected from an optical system is derived by multiplying the product of the Mueller matrices of its components with the Stokes vector representation of light input $\mathbf{S_{in}}$. The resultant output Stokes' vector $\mathbf{S_{out}}$ can then be analyzed to determine the intensity, degree of polarization and state of polarization of the emergent beam.

A. Mueller matrix model of the human eye

In the present study the polarization optics of the human eye relevant to HB is represented by the Stokes/Mueller formulation:

$$\mathbf{S}_{out}[x, y, k_1, k_2, \phi, \alpha, \varepsilon] = \mathbf{M}_M[x, y, k_1, k_2]\mathbf{M}_R[\phi, \alpha]\mathbf{S}_{in}[\varepsilon]$$

(1)

Linear polarized light with **e**-vector azimuth ε entering the system is defined by the Stokes vector $\mathbf{S_{in}}[\varepsilon]$. This is incident first on the cornea and then other refracting structures of the eye, which combined act as a retarder represented by the Mueller matrix $\mathbf{M_R}[\phi, \alpha]$, where ϕ is the magnitude of retardation and α is the azimuth of principle (slow) axis. Ocular retardation is predominantly due to corneal birefringence [21] and is assumed to be uniform along the visual axis [25]. Corneal retardation transforms the state of incident polarization (e.g. from linear to elliptical) depending on ϕ and the orientation of α relative to ε. It is assumed that there are no depolarizing effects due to, for example, light scatter, and that the stimulus is a homogenously illuminated polarized light field illuminating the macular area. As such, the refractive optics of the eye need not be considered.

After passing through the ocular refracting structures, the polarized light is then incident on the retina where it undergoes selective absorption within the region of the macula. The spatially-dependent light transmission properties of the macula are represented by the Mueller matrix $\mathbf{M_M}[x, y, k_1, k_2]$ which, in this case, acts as a radial diattenuator. The diattenuation (D) of an optical component is the dependence of the intensity transmittance of the exiting beam on the polarization state of the incident beam. It is quantified by the ratio of absolute difference to the sum of the orthogonal major (maximum) and minor (minimum) transmittances k_1, k_2, such that $0 \leq k_2 < k_1 \leq 1$ and $D = (k_1 - k_2)/(k_1 + k_2)$ [26]. In this model k_1, k_2 are, respectively, radially and tangentially orientated about a central point that coincides with the centre of the macula and is the origin (x = 0, y = 0) of a Cartesian coordinate system. In previous studies [18-20] the macula was assumed to act as a perfect polarizer/analyzer ($k_1 = 1$ and $k_2 = 0$), while the current model allows any transmittance values. Note that the macula has intrinsic birefringence, with radially symmetric principle axes of retardation aligned with principle transmittances [27]. This configuration has no effect on polarization state in the configuration investigated in this study and as such macular birefringence is ignored in the present model.

After passing through the macula, the state of polarization of light incident on the photoreceptors is defined by the Stokes' vector $\mathbf{S_{out}}$ at a point (x, y). Human photoreceptors do not differentially respond to polarization state under normal physiological conditions of illumination parallel to the receptor long axes [28]: it is therefore here only necessary to consider the first (intensity) component of the output Stokes' vector (S_0). Examples of the mathematical method are detailed elsewhere [19].

B. The HB model

Evaluating Eq. (1) for the output of the first Stokes' parameter allows an expression to be derived for the intensity of light reaching the photoreceptors, the light transmission function (T_H), such that

$$T_H(x, y, k_1, k_2, \phi, \alpha, \varepsilon) =$$
$$1 - \frac{D(x, y)}{2(x^2 + y^2)}\begin{bmatrix}(2 - k_1 - k_2)(x^2 + y^2) \\ + (k_1 - k_2)\begin{bmatrix}\cos\phi\sin(2(\alpha - \varepsilon))(\sin2\alpha)(y^2 - x^2) - 2xy\cos(2\alpha)) \\ + \cos(2(\alpha - \varepsilon))(\cos2\alpha)(y^2 - x^2) + 2xy\sin(2\alpha))\end{bmatrix}\end{bmatrix}$$

(2)

Where $D(x, y) \in \{0, 1\}$ is a density function that modulates T_H in two-dimensional space..

C. The density function and macular pigment density

The density function describes the density and two-dimensional distribution of the region of the macula that absorbs polarized light. In previous models this was assumed to be uniform and boundless ($D(x, y)$ = 1, Figure 1a). For the present study, the density function is assumed to correspond to the distribution of macular pigment optical density (MPOD), although any other mathematically defined function can be used.

The distribution of macular pigment varies considerably in magnitude and extent between individuals [29], but several patterns are consistent [30] and five categories (A – E) are described [31]. Category A (11% of cases in Sharifzadeh *et al*'s study) has very low MPOD and will not be considered here. In the majority of individuals MPOD declines monotonically as a function of distance from the foveal centre (Sharifzadeh *et al*'s categories B (22%), C (28%), E (12%)). Some data fit an exponential model (category C) in which MPOD is half the central (maximum) value at 1° – 2°, and is undetectable from 6 – 8° eccentricity [29]. In other individuals there is a bimodal distribution with a central maximum surrounded by an annular plateau (category B) or second annular peak from 0.5° to 1.0° eccentricity [32] (category D (17%)). A further variant [32] has a central 'dip' of reduced density surrounded by an annulus where density exceeds the central value (here categorised D1). Macular pigment profiles are assumed to have approximately radial symmetry [29] [33], although irregular patterns occur *in vivo*.

The macular pigment density (MPD) model used here (Equation 3) is based on the one-dimensional model of Berendschot and van Norren [32]. This is extended to two-dimensional Cartesian (x, y) space, and comprises an eccentricity-dependent exponential decline (with coefficient A_1) and a varying Gaussian component (with coefficient A_2); the other parameters are defined together with physiological ranges in Table 1.

$$\mathrm{MPD}(x, y) = A_1 10^{-\rho_1\sqrt{x^2 + y^2}} + A_2 10^{-\rho_2(\sqrt{x^2 + y^2} - x_2)^2}$$

(3)

The density function of the present study is the normalized form of Equation 3.

D. Dichroic ratio and principal transmittances

The dichroic ratio (G) is the ratio of major to minor principle transmittances (k_1/k_2) [15]. A mean value of $\log_{10} G = 0.054$ (range 0.018 – 0.082) at a wavelength of 457.8 nm was determined for seven human eyes *in vivo* using a method based on the perception of HB [34]. Assuming no extinction for polarized light parallel to the preferred orientation of the pleochroic elements ($k_1 = 1$), the above values of G give a mean value of $k_2 = 0.88$ (range 0.83 - 0.96).

Table 1 Parameters and variables defining MPD

Parameters*		Value range*	Category values†				
			B	C	D	D1	E
A_1	amplitude of the exponential component	0.28±0.13 (reflectance)	0.25	0.3	0.3	0.25	0.2
A_2	amplitude of the Gaussian component	0.13±0.07 (reflectance)	0.1	0.045	0.15	0.2	0.12
ρ_1	Peakedness of the exponential component	0.38±0.24°	0.3	0.5	0.15	0.3	0.22
ρ_2	Peakedness of the Gaussian component	1.2±1.1 deg²	0.6	0.1	1.2	1.2	0.3
x_2	x-axis eccentricity at which the Gaussian distribution peaks	0.70±0.66°	1.3	0.7	1.3	1.3	1.2
x, y	Cartesian coordinates of eccentricity relative to centre of macula / radial diattenuator						

* from Berendschot and van Norren [32]

† derived to fit the categories of Sharifzadeh, Bernstein and Gellermann [31]

E. Corneal Retardation

Birefringence, and hence retardation, is variable and complex across the extent of the cornea [21]. The central cornea, which is that part relevant to the generation of HB, behaves as a simple uniform retarding plate. Comprehensive studies of corneal retardation [25, 35] identify extensive inter-individual variability with retardances ranging from 0 – 100 nm, with 'most subjects' falling between 20 – 70 nm. The slow axis of retardation is typically 10° – 20° from the horizontal in a superotemporal to inferonasal direction. Eyes are approximately mirror symmetric. Whilst the methods of these studies use wavelengths exceeding those at which HB are perceived, comparable results have been obtained using HB detection [15, 36]. In the present study a typical cornea is assumed to have a central retardation of 50 nm (ϕ = 0.11λ at 460 nm) with the slow axis of retardation directed 15° nasally downwards. A central retardation of 100 nm (ϕ = 0.22λ at 460 nm) is taken as a maximum physiological value [37].

F. Simulating HB

It is now possible to simulate the appearance of HB using the 2-dimensional radial diattenuator model (Equation 2) and the MP density function (normalized Equation 3), given appropriate macular density parameters (Table 1). Computational analysis and graphics generation were performed using *Mathematica* (Wolfram Research, Inc., Champaign, IL, Version 11.1.1.0, (2017)). The method is demonstrated stepwise in Figure 1, where it is assumed that there is negligible effect of ocular retardation. Simulated HB intensity for a uniform (D(x, y) = 1), perfect (k_1 = 1, k_2 = 0) radial diattenuator is shown in Figure 1a. This is identical to the image generated by previous models: note that there is no boundary to the extent of this figure.

A density function derived from parameters for model D1 (Table 1) is shown as a two dimensional density plot in Figure 1b. The effect of the density function of (b) on the radial diattenuation model (a) is shown in Figure 1c, where the form and intensity of the image is highlighted with contours of 0.75 (75%, outer), 0.5 (50%) and 0.25 (25%, inner) transmission (isotransmission contours). The isotransmission contours have a lobate pattern and are a useful means of outlining the morphology of an otherwise diffuse image. The horizontal and vertical maxima of a given contour give a simple metric for the radial and circumferential extent ('length' and 'width') of different simulations; for example, the 0.75 (75%) transmission contour of Figure 1c has a length $L_{0.75}$ = 2.1° and width $W_{0.75}$ = 1.2°.

Introducing realistic values of principal transmittances (k_1 = 1, k_2 = 0.88) generates the image shown in Figure 1d, which demonstrates the faintness and low contrast of HB.

Animations of static images simulate the effects of incident linear polarization rotating with a constant angular velocity (see Supplementary Material visualizations 1 - 5). In particular, the animated simulations demonstrate the effect of different retardation values (0 λ, 0.11 λ, 0.22 λ, 0.25 λ) on kinetic HB contrast, and the orientation of HB relative to incident polarization.
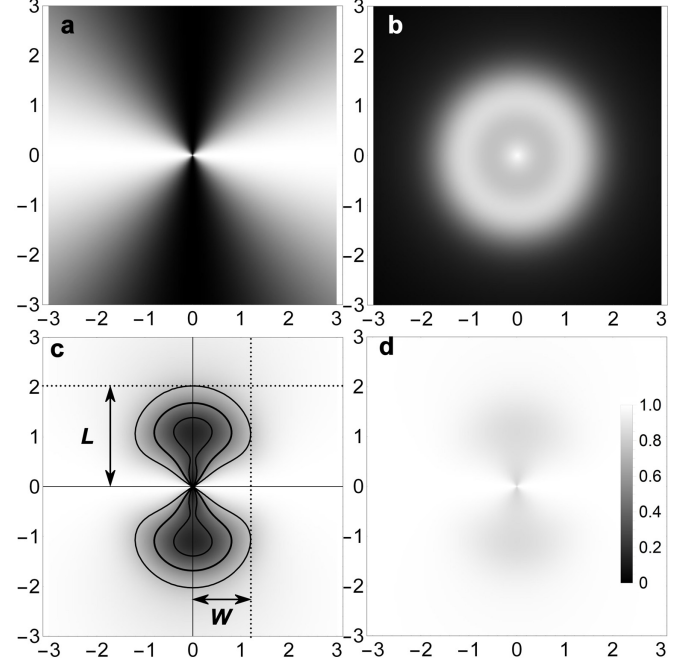

Figure 1 Components of the HB model for incident linear polarized light with horizontal orientation (ε = 0). (a) Radial diattenuator (RD) simulation (k_1 = 1, k_2 = 0); (b) uniform density function $D(x, y)$ = 1. Density function for macular pigment density model D1. (c) Radial diattenuator simulation (k_1 = 1, k_2 = 0) with density function D with superimposed 0.75 (outer), 0.50, 0.25 (inner) isotransmission contours. The outer 0.75 contour is used here to define length (L) and width (W) parameters. (d) HB simulation as in (c) but with principal transmittances k_1 = 1, k_2 = 0.88. Horizontal and vertical scales are degrees eccentricity from the centre of RD/macula. The greyscale indicates transmission for a, c, and d, and normalized density for b.

3. Results

The relationship between the five categories of circularly symmetric macular pigment density and HB morphology for horizontal linear polarized light ($\varepsilon = 0$) is shown in Figure 1 (Category D1) and Figure 2 (Categories B, C, D, E). In both figures, the MPD function is compared to the radial diattenuator simulation, perfect diattenuation ($k_1 = 1$, $k_2 = 0$) and a HB simulation with representative physiological diattenuation ($k_1 = 1$, $k_2 = 0.88$).

Variation between simulations is evident in the density and contour plots. The exponential model (C) attenuates rapidly from the central peak and gives rise to a radial diattenuator simulation that is also rapidly radially attenuating and narrow ($L_{0.75} = 1.8°$, $W_{0.75} = 0.7°$): the corresponding HB simulation is faint, narrow and with diminished radial extent. The simulations are more radially extensive and broader for the central plateau models B ($L_{0.75} = 2.4°$, $W_{0.75} = 1.3°$), D, D1 ($L_{0.75} = 2.2°$, $W_{0.75} = 1.3°$), and E ($L_{0.75} = 3.1°$, $W_{0.75} = 1.6°$). The ring model (D1) is centrally attenuated. The lobate pattern is hour-glass-shaped for B, C and E, but is pinched centrally in D and D1.

The effect of decreasing diattenuation (i.e. Increasing k_2, with $k_1 = 1$, $k_2 = 0.75, 0.83, 0.88, 0.96$) on HB morphology is shown in Figure 3 for a category E MPD and horizontal incident linear polarization ($\varepsilon = 0$). Isotransmission contours are now appropriate for the range of transmission ($T_H = 0.75 – 1$) at 0.9625 (outer), 0.925, 0.8875 (inner): the 0.9625 isotransmission contour is used as the index for the length ($L_{0.9625}$) and width ($W_{0.9625}$) parameters. Maximum brush contrast (Michelson contrast) is equated to diattenuation ($C = D = (k_1 – k_2)/(k_1 + k_2)$). The width and length of the brushes constrict ($L_{0.9625}$ and $W_{0.9625}$ diminish), and contrast/diattenuation falls with increasing k_2.

A further set of simulations (Figure 4) demonstrate the effect of physiological values of ocular retardation ($\phi = 50$ nm and 100 nm at $\alpha = 15°$ for an observation wavelength $\lambda = 460$ nm) on the morphology of HB for different incident **e**-vector orientations. As before, the simulation uses a category E MPD and diattenuations $k_1 = 1$, $k_2 = 0.88$. The simulations of Figure 4 are for incident linear polarization orientations $\varepsilon = 0°$ ($\alpha – 15°$), $15°$ (α), $37.5°$ ($\alpha + 22.5°$), $60°$ ($\alpha + 45°$).

A typical physiological retardation of $\phi = 50$ nm, $\alpha = 15°$, has little discernible effect on the appearance of HB (Figure 4 left two columns; Supplementary Material visualization 2). As the retardation magnitude increases above this value, the non-linear relationship between the orientations of incident polarization and HB orientation and contrast become increasingly apparent up to $\phi = \lambda/4$. Thus for the high physiological value of $\phi = 100$ nm (0.22λ), there is a non-linear cyclical contrast change and variable disparity between ε and orientation of the brushes (Figure 4 right two columns; Supplementary Material visualizations 3, 4). Greatest kinetic non-linearity is seen with a retardation of one quarter of the operating wavelength ($\phi = 115$ nm = $\lambda/4$ at 460 nm, see Supplementary Material visualization 5) when the brushes alternate in alignment with the fast/slow axes of the retarder, and their contrast modulates such that it is maximum when the $\varepsilon = \alpha$ and $\varepsilon = \alpha + 90°$ (i.e. incoming linear polarization is aligned with one of the retarder axes) and zero when $\varepsilon = \alpha \pm 45°$ (incoming linear polarization 45° to the retarder axes).
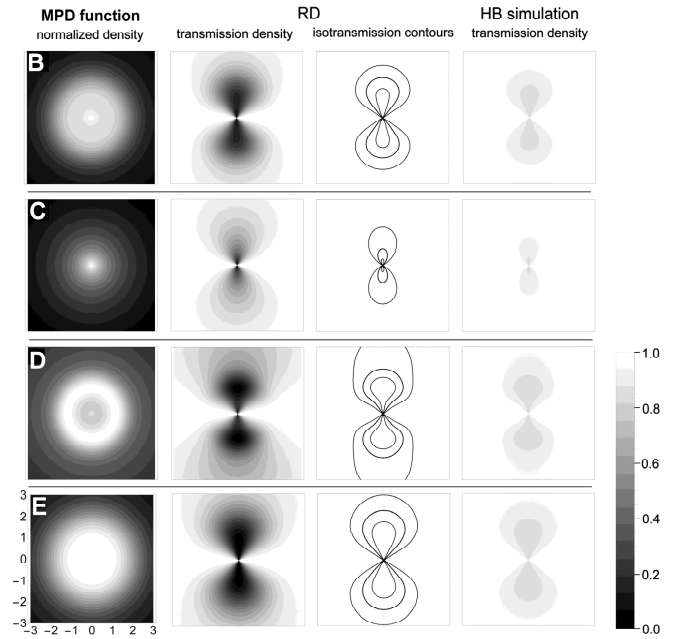

Figure 2 Macular pigment density (MPD function), radial diattenuator (RD) and Haidinger's brushes (HB) simulations for MPD categories B, C, D and E. Conditions of simulations and scales as in Figure 1. Horizontal/vertical scale (bottom left) is degrees eccentricity from centre of RD/macula; greyscale is transmission for RD and HB, and density for MPD function.
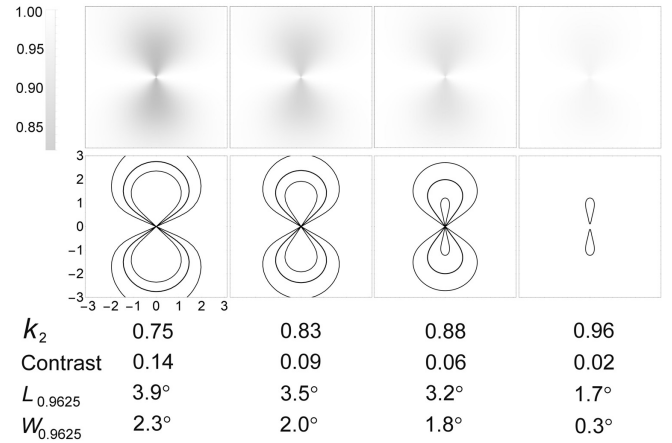

k_2	0.75	0.83	0.88	0.96
Contrast	0.14	0.09	0.06	0.02
$L_{0.9625}$	3.9°	3.5°	3.2°	1.7°
$W_{0.9625}$	2.3°	2.0°	1.8°	0.3°

Figure 3 HB simulations for physiological diattenuations.

Density graphics are for transmission range $T_H = 0.75 – 1.00$; isotransmission contours are at 0.9625 (outer), 0.9250, 0.8875 (inner); $k_1 = 1$, $k_2 = 0.75, 0.83, 0.88, 0.96$; $\varepsilon = 0$. Note that for the $k_2 = 0.96$ simulation only the outer 0.9625 isotransmission contour is present. Length and width parameters for the 0.9625 isotransmission contours ($L_{0.9625}$, $W_{0.9625}$) and contrast are as indicated

$\phi = 50\text{nm}$ $\phi = 100\text{nm}$

$\varepsilon = 0°,\ \alpha = 15°$

$\varepsilon = \alpha = 0°$

$\varepsilon = 37.5° = \alpha + 22.5°$
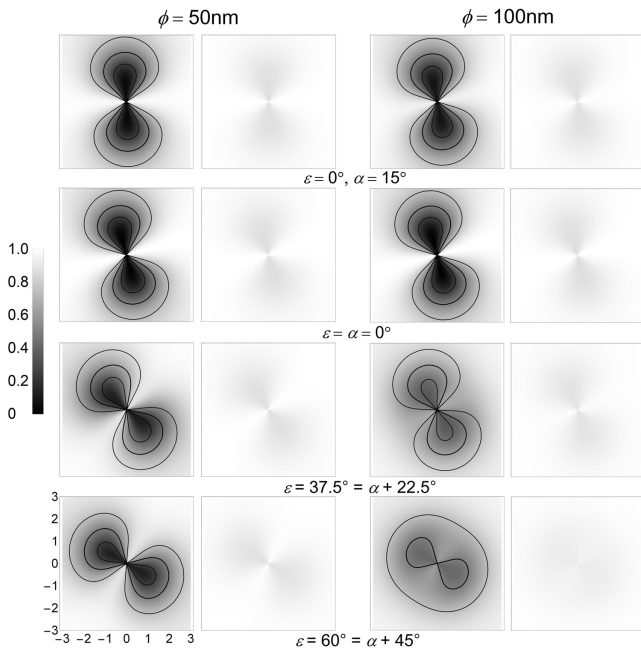
$\varepsilon = 60° = \alpha + 45°$

Figure 4 RD and HB simulations with retardation and rotating incident polarization. HB simulation for right eye: corneal retardation $\phi = 50$, 100 nm; azimuth nasally downward ($\alpha = 15°$), $k_1 = 1$, $k_2 = 0.88$. Category E MPD function for **e**-vector rotating between $\varepsilon = 0°$ and $\varepsilon = 60°$. Scales as in Figure 2.

4. Discussion

Haidinger's brushes were first described in the literature over 150 years ago [1], and while they have been depicted loosely as taking the form of a bushel of wheat, bow-tie, figure of eight, hour glass and propeller, among others, none of these descriptions seems to adequately do justice to the fact that everyone experiences their very own perception of the effect due to the physiological nature of the underlying mechanism. The model presented herein provides, for the first time, a comprehensive analysis of the various physiological parameters that alter the unique personal perception of HB, integrating the variable effects of corneal birefringence, macular pigment density and macular pigment distribution patterns. The resulting range of possible perceptions that can be calculated is highly variable and highlights just how different the experience can be among individuals.

The model is based on the accepted hypothesis [2] that the macula behaves as a radial diattenuator centred at the foveola and, unlike previous models [18-20], it incorporates a density function that describes the spatial density distribution of diattenuating elements within the macula. In addition, the model incorporates diattenuation and ocular retardation; parameters known to affect the morphology and dynamics of HB *in vivo*. The model can generate both static and dynamic representation of HB for any mathematically defined macular pigment spatial density function. Isotransmission contours are used as a metric for the morphology and perceived intensity of HB. The radial and circumferential maxima of a chosen index isotransmission contour serve as parameters for the length and width of HB.

An additional component of this study was the definition of a two-dimensional MPD function by modifying an existing one-dimensional model [32]. The normalized MPD function is then used as the density function defining the spatial distribution of macular pigment according to experimentally determined parameters. It assumes a circularly symmetrical distribution but can be adapted to accommodate real distribution patterns, which have been reported to vary from symmetry [33].

Absolute values of macular pigment, here quantified by the diattenuation parameters, also determine both the visibility and the appearance of HB, as demonstrated in the density plots and isotransmission contours in Figure 3. Thus for any particular MPD profile, high overall MP densities (low k_2 values) generate darker (higher contrast), wider and longer brushes than lower MP densities (higher k_2).

In reality, the radial extent of HB is determined both by macular pigment density and the areal extent of Henle fibre density. Thus a more accurate density function will take both factors into account, but this will require more detailed data regarding Henle fibre geometry than is available at present. The assumption of the present study that MPD is the principle determinant of HB morphology is reasonable given the known association between MP and the Henle fibre layer [38]. The model, however, is general and can readily incorporate a redefined density function as required.

Simulation results show the effect on HB of varying spatial distributions of MP (Figure 1, Figure 2). Different density functions affect radial (length) and circumferential (width) extent of HB (e.g. Figure 2 compare C and E) and HB morphology (e.g. Figure 2 compare C and D1). The known inter-individual variation in MP distribution [39] [29] is therefore a factor to be included when considering the variation in perception of HB. When corneal retardation is varied, the model generates animated HB simulations that demonstrate the variance in the dynamic aspects of HB behaviour for individuals with different corneal retardation (both optical thickness and orientation of the optical slow axis of retardation). The effect on the perception of HB when observing a rotating polarized light field can vary from HB rotating smoothly through 360° to only brief glimpses of the brushes in quadrants aligned with retardation axes (see Supplementary Material visualizations 3 – 5).

The effects of ocular retardation on HB contrast and relative orientation are well known, having been modelled theoretically [20] and demonstrated experimentally [36]. The equations of previous authors using different methods [18-20] can all be derived from simplifications of Equation 2, supporting the validity of the present model. There are several particular observations with respect to retardation that arise from the present study. For typical corneal retardations ($\phi \le 0.11\lambda$), the effect on HB appearance and dynamics is minimal (Figure 4 left two columns, see Supplementary Material visualization 2). The changes in contrast and non-linear relationship between orientation of HB and orientation of incident **e**-vector become increasingly evident with higher retardations (e.g. Figure 4 right two columns, see Supplementary Material visualizations 3, 4). It should be noted, however, that such high values only occur in a minority of subjects. For most individuals, retardation is considerably less ($\phi < 70$ nm $= 0.15\lambda$) [25, 35].

This study demonstrates that variations in (1) diattenuation (here related to total macular pigment density), (2) the spatial distribution of diattenuation (described by the density function and related to macular pigment spatial distribution) and (3) the retardation properties of the ocular media all contribute to the perceived appearance of HB. These factors all show considerable *in vivo* inter-subject variability and are sufficient to account for the known inter-subject and inter-ocular variability in the perception of HB.

Photography of the macula with polarized light generates a 'Maltese cross' or brush-like pattern that has been proposed as an objective equivalent to HB [40, 41]. However, this 'macular cross' phenomenon differs from HB in its spectral characteristics, form and behavior, and probably results from macular radial birefringence [42]. To date, objective imaging of HB has not been possible because of its entoptic

nature. Pictorial representations of HB have either been subjective artistic impressions of variable accuracy, or simple unbounded computer graphic simulations similar to Figure 1a. The static and animated graphical representations of HB presented in this study are proposed as realistic simulations of the observed appearance and behaviour of HB. Thus, apart from utility in the theoretical exploration of HB, these representations are also useful for educational, illustrative and demonstration purposes.

Quantitative studies of HB have derived information about macular pigment density [5, 15-17] and ocular retardation [16, 36]. These have clinical relevance in that macular pigment density and distribution is affected by macular disease, and inter-observer variations in ocular retardation may act as a confounding variable in any qualitative or quantitative clinical assessment. The model assumes that there are no depolarization effects. Depolarization due to light scatter, particularly from lens opacities and other inhomogeneities of the ocular media, may affect the perception of HB. Therefore, the effects of media opacities, especially in the elderly, require further study. The clinical applications of HB are subjects of current research, particularly with respect to quantifying macular pigment density and diagnosis of macular disease [17]. The model presented in this study further enhances the theoretical foundation for these and future investigations.

5. References

1. W. Haidinger, "Ueber das directe Erkennen des polarisirten Lights und der Lage der Polarisationsebene," Annalen der Physik und Chemie **63**, 29-39 (1844).
2. J. McGregor, S. E. Temple, and G. Horváth, "Human Polarization Sensitivity," in *Polarized Light and Polarization Vision in Animal Sciences,* 2 ed., G. Horváth, ed. (Springer, Heidelberg, 2014), pp. 303 - 315.
3. W. Haidinger, "Ueber complementäre Farbeneindrücke bei Beobachtung der Lichtpolarisationsbüschel," Annalen der Physik und Chemie **67**, 435-437 (1846).
4. H. d. Vries, A. Spoor, and R. Jielof, "Properties of the eye with respect to polarized light," Physica **19**, 419-432 (1953).
5. E. J. Naylor and A. Stanworth, "Retinal pigment and the Haidinger effect," J Physiol **124**, 543-552 (1954).
6. W. Haidinger, "Dauer des Eindruckes der Polarisationsbüschel auf die Netzhaut," Annal Physik **93**, 318 (1854).
7. G. Boehm, "Über maculare (Haidinger'sche) Polarizationsbüschel und über eine polarizationsoptischen Fehler der Auges," Acta Ophthalmol **18**, 109-142 (1940).
8. C. C. Shute, "Haidinger's brushes and predominant orientation of collagen in corneal stroma," Nature **250**, 163-164 (1974).
9. W. Haidinger, "Beobachtung der Licht-Polarisations-Büschel auf Flächen, welche das Licht in zwei senkrecht auf einander stehenden Richtungen polarisiren," Annalen der Physik und Chemie **46**, 305-319 (1846).
10. J. C. Maxwell, "Manuscript on experiments on the cause of Haidinger's brushes," in *The scientific letters and papers of James Clerk Maxwell* (Taylor and Francis, London, 1850), pp. 199 - 204.
11. H. Helmholtz, *Treatise on Physiological Optics,* 3rd German Edn. ed. (Optical Society of America, 1924), Vol. 2, pp. 304 - 308.
12. M. Goldschmidt, "A new test for function of the macula lutea," Archives of Ophthalmology **44**, 129-135 (1950).
13. H. W. Forster, "The Clinical Use of the Haidinger's Brushes Phenomenon," American journal of ophthalmology **38**, 661-665 (1954).
14. A. Stanworth and E. J. Naylor, "The measurement and clinical significance of the Haidinger effect," Trans Ophth Soc U.K. **75**, 67-79 (1955).
15. R. A. Bone, "The role of the macular pigment in the detection of polarized light," Vision Res **20**, 213-220 (1980).
16. R. A. Bone and J. T. Landrum, "Macular pigment in Henle fiber membranes: a model for Haidinger's brushes," Vision Res **24**, 103-108 (1984).
17. P. L. Muller, S. Muller, M. Gliem, K. Kupper, F. G. Holz, W. M. Harmening, and P. Charbel Issa, "Perception of Haidinger Brushes in Macular Disease Depends on Macular Pigment Density and Visual Acuity," Invest Ophthalmol Vis Sci **57**, 1448-1456 (2016).
18. G. P. Misson, "Form and behaviour of Haidinger's brushes," Ophthal Physiol Opt **13**, 392-396 (1993).
19. G. P. Misson, "A Mueller matrix model of Haidinger's brushes," Ophthal Physl Opt **23**, 441-447 (2003).
20. M. Rothmayer, W. Dultz, E. Frins, Q. Zhan, D. Tierney, and H. Schmitzer, "Nonlinearity in the rotational dynamics of Haidinger's brushes," Appl. Opt. **46**, 7244-7251 (2007).
21. L. J. Bour, "Polarized light and the eye," in *Visual Optics and Instrumentation*, W. N. Charman, ed. (Macmillan Press, New York, 1991), pp. 310-325.
22. D. H. Goldstein, *Polarized Light, Third Edition* (CRC Press, 2010).
23. E. Collett, *Polarized Light. Fundamentals and Applications* (Marcel Dekker, New York, 1993).
24. W. A. Shurcliff, *Polarized Light: Production and Use* (Harvard University Press, Cambridge, Massachusetts, 1962).
25. R. W. Knighton and X. R. Huang, "Linear birefringence of the central human cornea," Invest Ophthalmol Vis Sci **43**, 82-86 (2002).
26. J. M. Bueno and P. Artal, "Average double-pass ocular diattenuation using foveal fixation," Journal of Modern Optics **55**, 849-859 (2008).
27. H. B. k. Brink and G. J. van Blokland, "Birefringence of the human foveal area assessed in vivo with Mueller-matrix ellipsometry," J Opt Soc Am A **5**, 49-57 (1988).
28. M. F. Land and D. E. Nilsson, *Animal Eyes*, Oxford Animal Biology Series (Oxford University Press, Oxford, 2002).
29. J. B. R. Hammond, B. R. Wooten, and D. M. Snodderly, "Individual variations in the spatial profile of human macular pigment," J. Opt. Soc. Am. A **14**, 1187-1196 (1997).
30. P. S. Bernstein, F. C. Delori, S. Richer, F. J. M. van Kuijk, and A. J. Wenzel, "The value of measurement of macular carotenoid pigment optical densities and distributions in age-related macular degeneration and other retinal disorders," Vision Research **50**, 716-728 (2010).
31. M. Sharifzadeh, P. S. Bernstein, and W. Gellermann, "Nonmydriatic fluorescence-based quantitative imaging of human macular pigment distributions," J Opt Soc Am A Opt Image Sci Vis **23**, 2373-2387 (2006).
32. T. T. Berendschot and D. van Norren, "Macular pigment shows ringlike structures," Invest Ophthalmol Vis Sci **47**, 709-714 (2006).
33. A. G. Robson, J. D. Moreland, D. Pauleikhoff, T. Morrissey, G. E. Holder, F. W. Fitzke, A. C Bird, and F. J. G. M. van Kuijk, "Macular pigment density and distribution: comparison of fundus autofluorescence with minimum motion photometry," Vision Research **43**, 1765-1775 (2003).
34. R. A. Bone and J. T. Landrum, "Distribution of macular pigment components, zeaxanthin and lutein, in human retina," Methods Enzymol **213**, 360 - 366 (1992).
35. R. N. Weinreb, C. Bowd, D. S. Greenfield, and L. M. Zangwill, "Measurement of the magnitude and axis of corneal polarization with scanning laser polarimetry," Arch Ophthalmol **120**, 901-906 (2002).
36. S. E. Temple, J. E. McGregor, C. Miles, L. Graham, J. Miller, J. Buck, N. E. Scott-Samuel, and N. W. Roberts, "Perceiving polarization with the naked eye: characterization of human polarization sensitivity," Proc. R. Soc. B **282**, 20150338 (2015).
37. R. W. Knighton, X. R. Huang, and L. A. Cavuoto, "Corneal birefringence mapped by scanning laser polarimetry," Optics express **16**, 13738-13751 (2008).
38. M. Trieschmann, F. J. G. M. van Kuijk, R. Alexander, P. Hermans, P. Luthert, A. C. Bird, and D. Pauleikhoff, "Macular pigment in the human retina: histological evaluation of localization and distribution," Eye **22**, 132-137 (2008).
39. B. J. Hammond and K. Fuld, "Interocular differences in macular pigment density," Invest Ophthalmol Vis Sci **33**, 350-355 (1992).
40. B. F. Hochheimer, "Polarized light retinal photography of a monkey eye," Vision Res **18**, 19-23 (1978).

41.   B. F. Hochheimer and H. A. Kues, "Retinal polarization effects," Appl Optics **21**, 3811-3818 (1982).

42.   A. E. Elsner, A. Weber, M. C. Cheney, and D. A. Vannasdale, "Spatial distribution of macular birefringence associated with the Henle fibers," Vision Res **48**, 2578-2585 (2008).